









Temperature effect on the porosity of hydroxyapatite scaffolds and its use in tissue engineering

Efecto de la temperatura sobre la porosidad de andamios de hidroxiapatita y su uso en ingeniería de tejidos

Vareska Lucero Zarate-Córdova¹ , Mercedes Teresita Oropeza-Guzmán² , Eduardo Alberto López-Maldonado³ , Ana Leticia Iglesias¹ , Theodore Ng⁴, Eduardo Serena-Gómez⁵, Graciela Lizeth Pérez-González^{1,3} , Luis Jesús Villarreal-Gómez^{1,3} 

¹Facultad de Ciencias de la Ingeniería y Tecnología, Universidad Autónoma de Baja California, Tijuana, Baja California, México.

²Centro de Graduados, Instituto Tecnológico de Tijuana, Tijuana, Baja California, México.

³Facultad de Ciencias Químicas e Ingeniería, Universidad Autónoma de Baja California, Tijuana, Baja California, México.

⁴Oakland Oral and Maxillofacial Surgery, Oakland, California, United States.

⁵Facultad de Ciencias de la Salud, Universidad Autónoma de Baja California, Tijuana, México.

Corresponding author: Dr. Luis Jesús Villarreal Gómez, Facultad de Ciencias de la Ingeniería y Tecnología, Universidad Autónoma de Baja California, Tijuana, México. Blvd. Universitario #1000. Unidad Valle de las Palmas. Tijuana, Baja California, México. Postal Code: 22260. E-mail: luis.villarreal@uabc.edu.mx. ORCID: 0000-0002-4666-1408.

Recibido: 8 de Septiembre del 2020

Aceptado: 27 de diciembre del 2020

Publicado: 28 de Diciembre del 2020

Abstract. – *The search for a suitable bone replacement is of great importance due to the difficulty to use autologous transplants. Hence, the objective of this work is to compare the temperature effect on the porosity and average pore diameter of hydroxyapatite porous scaffolds fabricated by the salt leaching method. Hydroxyapatite porous scaffolds fabricated by the salt leaching technique were sintered from ~150 to 1000 °C. Synthesized hydroxyapatite was assessed by X-ray diffraction (XRD). Zeta potential at different temperatures was evaluated. Specimens were characterized using scanning electron microscopy (SEM) and Raman analysis. The results showed that significant porosity (57%) and pore size (49 μm) occurred with a thermal treatment above ~ 850 °C for scaffolds that were pre-sintered at 1050 °C.*

Keywords: Hydroxyapatite; porous scaffold; salt leaching method.

Resumen. - *La búsqueda de un reemplazo óseo adecuado es de gran importancia debido a la dificultad de utilizar trasplantes autólogos. Es por esto, que el objetivo de este trabajo es comparar el efecto de la temperatura sobre la porosidad y el diámetro promedio de poro fabricados con el método de lixiviación de sales, siendo sinterizados desde ~150 a 1000 °C. Los andamios fabricados de hidroxiapatita fueron evaluados con difracción de rayos X (XRD). El potencial zeta fue evaluado a diferentes temperaturas. Los especímenes fueron caracterizados utilizando microscopía electrónica de barrido (SEM) y análisis Raman. Los resultados mostraron que la porosidad importante (57%) y tamaño de poro (49 μm) ocurren con un tratamiento térmico superior a ~ 850 °C para andamios que fueron pre-sinterizados a 1050 °C.*

Palabras clave: Hidroxiapatita; andamios porosos; método de lixiviación de sales.

1. Introduction

In tissue engineering applications, autologous bone grafting procedure is the current treatment for bone injuries, but this procedure has several limitations, which include additional surgical procedures, chronic pain after surgery, donor site morbidity and lack of tissue availability [1]. To overcome the problems associated with autograft use, alloplastic materials have been developed. Alloplastics are materials with unlimited availability, no risk of disease transmission and osteoconductive properties [2]. The most common alloplastic material used in biomedical applications is hydroxyapatite [3].

The use of hydroxyapatite as porous scaffolds or as a bioactive coating material in medical devices is justified because ceramics resist oxidation and corrosion in the physiological environment and possess great resistance to friction and wear; however, hydroxyapatite by itself has poor biomechanical properties, its ability to withstand flexion and compression stresses is very low, causing it to fracture easily. Given these drawbacks, in recent decades several organic compounds of the extracellular matrix such as fibronectin, vitronectin, osteopontin, growth factors and type I collagen, among others, have been added to hydroxyapatite coatings in order to improve osteoconduction, cell adhesion and the mechanical properties of the coating [4-9]. A relatively new promising material that can improve the mechanical properties of the coating is graphene [10], since it has great flexibility and mechanical rigidity, in addition to its properties as an electrical conductor that could help coating methods based on voltage, such as electrodeposition and electrophoresis [11, 12].

It has been reported that the most suitable pore size for optimal vascularization is 100-500 μm , which also provides an area of adhesion to osteogenic cells [13, 14], and that percentage porosity values above 10% in ceramic materials indicate pore interconnectivity, the more

percentage of porosity, the more probability of pore interconnection. The porosity values present in trabecular bone vary between 30 and 90% with interconnected porosity between 50 and 90%. The more porosity and interconnectivity, the more ease of cell proliferation and migration, as well as greater nutrient transport [15].

The objective of this work is to compare the temperature effect on the porosity and average pore diameter of HAp porous scaffolds manufactured by the salt leaching method, where this technique is easy to perform, affordable and promotes the porosity of a compressed inorganic powder as hydroxyapatite.

2. Methodology

2.1. Materials

Distilled water (H_2O) (Arrowhead), 85% phosphoric acid (H_3PO_4), calcium hydroxide ($\text{Ca}(\text{OH})_2$) and potassium chloride (KCl) were obtained from Fermont and used as received.

2.2. Hydroxyapatite (HAp) synthesis

Hydroxyapatite powder (HAp) was synthesized using the methodology reported by Guillen-Romero, L, et al. [16], where an H_3PO_4 solution was blended with $\text{Ca}(\text{OH})_2$ w/v in a relation 1:1.67 with a constant stirring during 7 days. After that, the solution was washed 3 times by centrifugation at 3000 rpm for 5 min. The pellet was resuspended and filtered off through Buchner funnel and washed again with ethanol. The filtered sample was left to dry at 80 °C for 5 days in an oven. Finally, half a gram of the resulting HAp was sintered at four different temperatures (~150 °C, ~450 °C, ~850 °C and ~1000 °C) for 2 h to observe the influence of the temperature on the fabrication of the sintered hydroxyapatite (sHA) scaffolds [16, 17].

2.3. HAp and sHA porous scaffold preparation

Potassium chloride (KCl) was added to HAp and sHA in a KCl/HAp-sHA (1/1.85 w/w). The mixture was homogenized by grinding them together in a porcelain mortar. Then, the samples were compacted using a hydraulic press into cylindrical scaffolds with a force of 5000 lbs for 2 min. HAp and sHA scaffolds were sintered in different temperatures ranging from ~150 to 1000 °C for 2 h in an oven. Finally, HAp and pHA scaffolds were placed in a drip leaching system. The volume of liquid solvent used in the leaching process was 10 mL of distilled water for all samples. All sHA scaffolds disintegrated in contact with water during the drip leaching process. However, HAp scaffolds maintained their consistency. For this reason, the drip-leaching process was only applied to the HAp scaffolds [16, 18].

2.3. Analysis characterization

2.3.1. X-ray diffraction (XRD)

The equipment used for this analysis was the Bruker D8 Advance diffractometer, with the powder methodology. A metallic holder was used, and was set with few samples, enough to cover the surface of the holder (1 cm length x 3 mm width). After that, the holder was located inside the equipment with the following conditions: 15 and 30 rpm, lamp of copper (Cu) at 30 kV [16].

2.3.2. Raman spectroscopy

In the case of Raman spectroscopy, it was analyzed using an FRA 106/S FT-Raman, Bruker with an Nd: Y AG laser source operating at 1200 nm with a 180° back scattering geometry, spectral width 1 cm⁻¹, and power of the laser beam 250 mW reaching the sample [19].

2.3.3. Scanning electron microscopy (SEM)

Specimens were characterized by scanning electron microscopy (SEM). SEM images were obtained using secondary electron detector (SED). Percentage of porosity and average pore diameter were measured using the software Fiji ImageJ using images with a magnification of 1000 x.

2.3.4. Z potential studies

A Z potential analysis was performed using the HORIBA SZ-100 zetameter by taking 1 mg of the hydroxyapatite, 1 mmol of KCl and dissolving them in 100 mL of 70% ethanol using the BRANSONIC 2510R-MT sonifier. To determine the particle size, the same equipment was used with a solution of 10 mg in 100 mL of ethanol. Both Z potential and particle size analysis of HAp treated at different temperatures were also determined. For that, 1 gr of HAp, 0.001 mol of KCl and 100 mL of 70 % ethanol were used in order to make the Z potential analysis and 10 mL of HAp with 100 mL of ethanol were used in the particle size analysis. Misonix Branson 2510R-MT ultrasonic cleaner was used to mix the samples [16].

3. Results and Discussions

3.1. Raman spectroscopy

The Raman spectrum showed in figure 1, that the obtained signals are according with literature [16-18], demonstrating the HAp presence in the samples, validating its synthesis.

In the Raman spectra all signals were assigned to the internal vibrational modes of the PO₄⁴⁻ group. The intense signal at 960 cm⁻¹ matches with the symmetric stretching mode ν_1 of the tetrahedron PO₄⁻³ group (P-O bond); the weak peak around 600 cm⁻¹ is assigned to the triple bending mode ν_4 of PO₄⁻³ (O-P-O bond); the double degenerative bending mode ν_2 of the PO₄⁻³

group (O-P-O bond) can be observed as a medium peak at 440 cm^{-1} [19-21].

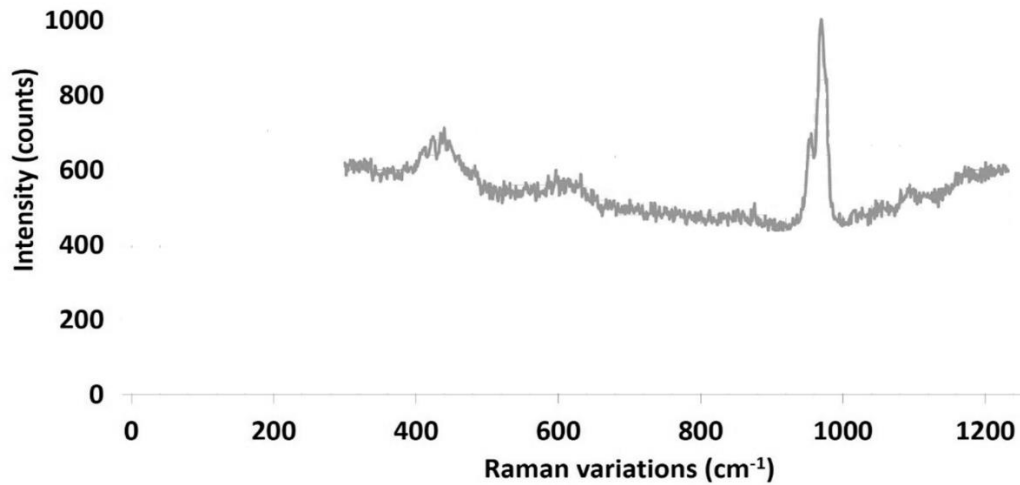


Figure 1. Raman spectrum of hydroxyapatite.

3.2. X-ray diffraction (XRD) analysis

Figure 2, shows the diffraction pattern, were 4 greater signals of intensity located at the left of the spectra between the angular zone $20 < 2\theta < 80$ were assigned corresponding to the Miller indexes of (002), (211), (112), (300) (red circle). Despite that those indices are attributed to

hydroxyapatite, the lack of separated signals with lower strength indicate a low crystallinity [18, 22, 23]. However, a comparison between the obtained HAp patterns with JCPDS 09-432 file shows that HAp obtained in this work represents the typical hydroxyapatite sign.

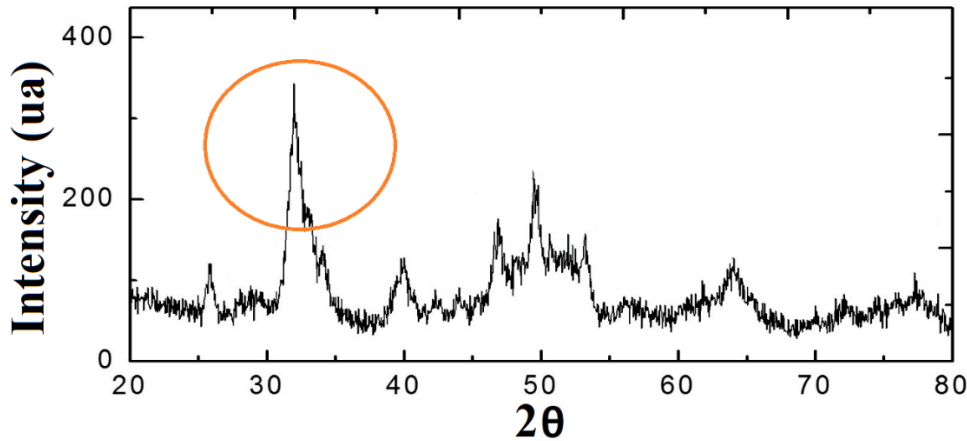


Figure 2. XRD spectrum of HAp. JCPDS 009-0432.

3.3. Scanning electron microscope (SEM)

The microstructure of HAp and sHA porous scaffolds was examined using scanning electron microscopy “figure 3 A-C” and “figure 3 E-G”

respectively. The heat treatment applied to HAp and sHA scaffolds were carried out using temperatures from ~ 150 to $1000\text{ }^\circ\text{C}$. Porosity and pore size were estimated using the ImageJ software “table 1”.

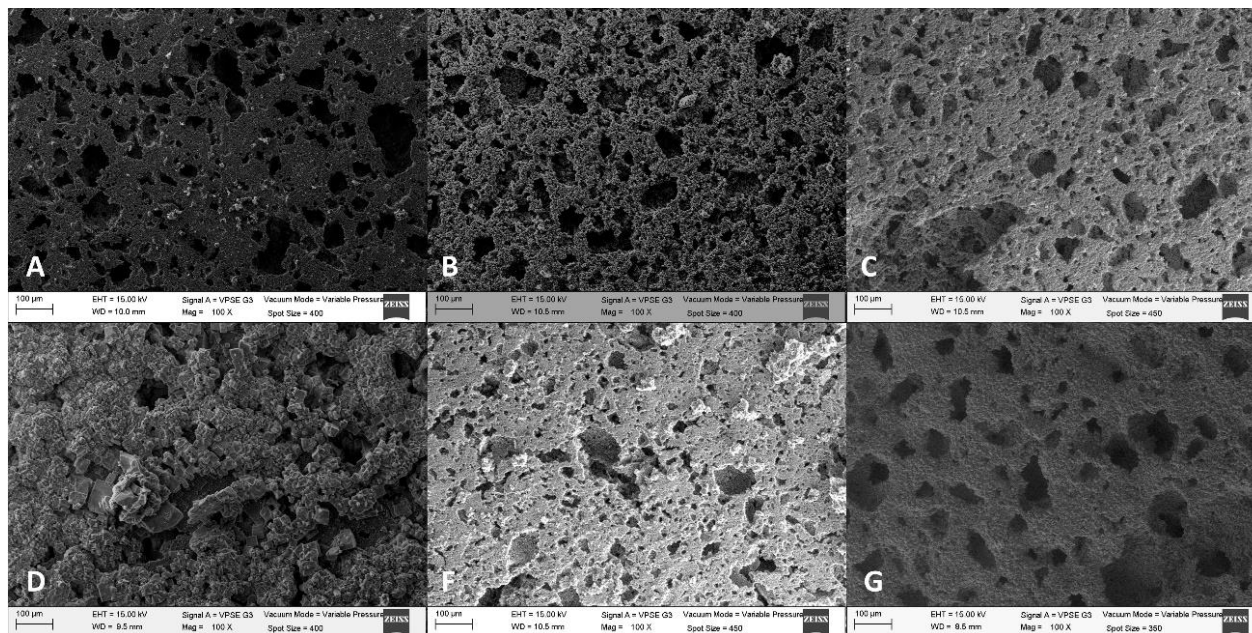


Figure 3. Micrographies of sHA scaffolds with different heat treatment for 2 hours at 15 KV of magnification. (A) ~150 °C at 2 h (B) ~850 °C at 2 h (C) ~1000 °C at 2 h (D) ~150 °C at 24 h (E) ~850 °C at 24 h (F) ~1000 °C at 24 h.

Table 1. Temperature effect on the porosity and average pore diameter of HA porous scaffolds. HAp (hydroxyapatite without sintering) sHA (hydroxyapatite sintered at 1000 °C).

Sample	Porosity %	Average pore diameter µm	Min	Max
HAp 150	13	70 ±41	25	169
HAp 850	57	43 ±37	10	248
HAp 1000	52	100 ±64	19	308
sHA 150	50	47 ±27	9	163
sHA 850	57	49 ±28	11	151
sHA 1000	49	48 ±34	9	186

“Table 1” shows the effect of temperature on the sHA. Porous scaffolds at ~150 °C produced less percentage of porosity than the other two sHA scaffolds exposed at ~850 and ~1000 °C. Both porosity and average pore diameter of HAp and sHA scaffolds treated at ~850 °C showed great similarity. A porosity of 57 % was obtained in HAp and sHA scaffolds treated at 850 °C.

Based on the results obtained by scanning electron microscopy, it is concluded that all specimens that were evaluated presented pore interconnectivity based in the fact that

percentage porosity in both HAp and sHA scaffolds were above 10 %. According to some studies, porosity values above 10 % indicate interconnectivity between pores in ceramic materials [22] and a higher porosity translates into higher cellular proliferation and nutrient transport.

In addition, microporosity and macroporosity was perceived in all samples. Pores between 9 and 308 µm were found. Sequeda reported that the most suitable pore size range for ease of cell

proliferation and migration varies between 100-500 μm [23].

Thermal treatment at higher temperature ($\sim 1000^\circ\text{C}$) of HAp scaffolds resulted in a

considerable increase of average pore diameter compared with the rest. It can be observed, that the particle size of HAp decreases when the temperature increment. The particle size results are shown in “table 2”.

Table 2. Particle size of hydroxyapatite (HA and HAS).

Sample	Particle size [μm]
No thermal treatment (HAp)	30 ± 3
sHA150 ($\sim 150^\circ\text{C}$)	12 ± 1
sHA450 ($\sim 450^\circ\text{C}$)	11 ± 0.4
sHA850 ($\sim 850^\circ\text{C}$)	11 ± 0.5
sHA1000 ($\sim 1000^\circ\text{C}$)	8 ± 0.2

Brown, C. et al., 2015, demonstrated that particle size its an important factor that impact stem cell differentiation through cell–cell and cell–matrix interactions [24]. With the thermal treatments of the sHA it was achieved a low particle size diameter ($\sim 8\text{-}12 \mu\text{m}$), which are interesting sizes for tissue engineering [24]. At $\sim 1000^\circ\text{C}$ where obtained the lowest particle size ($\sim 8 \mu\text{m}$). In the case of the particle size obtained ($\sim 30 \mu\text{m}$) from the HAp, its higher size can be attributed to the existence of coordinated H_2O molecules that remain when were allowed to dry at a temperature of $\sim 80^\circ\text{C}$. The particle size is suitable to use in coatings [16], because at a size of $10 \mu\text{m}$ allows cell adhesion, however, is not as feasible to be used in other medical applications, because the size of the particle would complicate

of the construction of seeding channels in the bone.

3.4. Z potential analysis

On the other hand, low zeta potentials values promote the differentiation of osteogenic cells at the surface’s material and negatively charged surfaces have excellent biocompatibility [25].

Table 3 show the lowest zeta potential results for HAp at higher temperature. At the opposing, the effect of heat temperature on HAp and sHA at $\sim 150^\circ\text{C}$ produced less percentage of porosity and higher zeta potential compared to ~ 850 and $\sim 1000^\circ\text{C}$ treatments. As a result, sHA scaffolds treated at $\sim 1000^\circ\text{C}$ can have potential properties for cell adhesion and proliferation [26-28].

Table 3. Z potential of Hydroxyapatite (HAp and sHA). Ethanol was used to prepared HA solutions for the Z potential analysis. All solutions were adjusted at pH of 7.5.

Sample	Z Potential [mV]	Electrophoretic movility [cm^2/Vs]	Conductivity [mS/cm]
No thermal treatment (HAp)	-18 ± 4	$-31 \cdot 10^{-6} \pm 7 \cdot 10^{-6}$	0.109
sHA150 ($\sim 150^\circ\text{C}$)	-19 ± 3	$-37 \cdot 10^{-6} \pm 7 \cdot 10^{-6}$	0.109
sHA450 ($\sim 450^\circ\text{C}$)	-22 ± 2	$-44 \cdot 10^{-6} \pm 3 \cdot 10^{-6}$	0.102
sHA850 ($\sim 850^\circ\text{C}$)	-15 ± 2	$-30 \cdot 10^{-6} \pm 5 \cdot 10^{-6}$	0.110
sHA1000 ($\sim 1000^\circ\text{C}$)	-27 ± 2	$-54 \cdot 10^{-6} \pm 4 \cdot 10^{-6}$	0.112

According to a study, the Z potential value for hydroxyapatite at this pH should be in the range of 15 mV as seen in the sintered sample at ~850 °C, however given the favorable results of the sample at ~1000 °C [16].

4. Conclusions

The porosity and average pore diameter of HA porous scaffolds fabricated by the salt leaching method can be controlled by thermal treatments. In this work, hydroxyapatite was successfully synthesized using the wet precipitation method. The higher porosity ratio was obtained at ~850 °C treatment, but lower Z potential of HAp was at ~1000 °C indicating that any of these two sHA sample can be adequate cell adhesion and proliferation properties. Further studies have to be done to find a balance with adequate % porosity and lower z potential.

Its important to denote, that all the obtained HAp and sHA scaffolds presented a superior porosity than 30 %, been suitable for trabecular bone replacement applications. Still, future tests are necessary to complement this study in order to propose these HAp and sHA scaffolds for tissue engineering applications.

5. Acknowledgments

The authors are grateful to Universidad Autónoma de Baja California, with the registered SICASPI-UABC project 351/2420. Moreover, the authors thanks to Alan Saul Alvarez Suarez for revision of the English in the manuscript.

References

[1] K. Yang et al., “ β -Tricalcium phosphate/poly (glycerol sebacate) scaffolds with robust mechanical property for bone tissue engineering,” *Mater. Sci. Eng. C*, vol. 56, pp. 37–47, Nov. 2015. <http://dx.doi.org/10.1016/j.msec.2015.05.083>.

[2] Z. Sheikh, C. Sima, and M. Glogauer, “Bone Replacement Materials and Techniques

Used for Achieving Vertical Alveolar Bone Augmentation,” *Materials*, vol. 8, no. 6. 2015. <http://dx.doi.org/10.3390/ma8062953>.

[3] J. Lindhe. *Periodontologia Clinica E Implantologia Odontologica. Médica Panamericana*; 2009. <https://books.google.com.mx/books?id=69zuJ1qspGwC>.

[4] L. J. Villarreal-Gómez et al., “Biocompatibility evaluation of electrospun scaffolds of poly (L-Lactide) with pure and grafted hydroxyapatite,” *J. Mex. Chem. Soc.*, vol. 58, no. 4, pp. 435–443, 2014. <http://dx.doi.org/10.29356/jmcs.v58i4.53>.

[5] G. Hannink and J. J. C. Arts, “Bioresorbability, porosity and mechanical strength of bone substitutes: What is optimal for bone regeneration?” *Injury*, vol. 42, pp. S22–S25, Dec. 2016. <http://dx.doi.org/10.1016/j.injury.2011.06.008>.

[6] C. T. I. Reviews, *Biomaterials Science, An Introduction to Materials in Medicine*. Cram101, 2016. <https://books.google.com.mx/books?id=TdrIAQAAQBAJ>.

[7] R. Bosco, J. Van Den Beucken, S. Leeuwenburgh, and J. Jansen, “Surface Engineering for Bone Implants: A Trend from Passive to Active Surfaces,” *Coatings*, vol. 2, no. 3. 2012. <http://dx.doi.org/10.3390/coatings2030095>.

[8] L. J. Villarreal-Gómez et al., *In vivo* biocompatibility of dental scaffolds for tissue regeneration, vol. 976. 2014. <http://dx.doi.org/10.4028/www.scientific.net/AMR.976.191>.

[9] K. Kuroda and M. Okido, “Hydroxyapatite Coating of Titanium Implants Using Hydroprocessing and Evaluation of Their Osteoconductivity,” *Bioinorg. Chem. Appl.*, vol. 2012, no. 1, pp. 1–7, 2012, doi: <http://dx.doi.org/10.1155/2012/730693>.

[10] C. Berger et al., “Ultrathin Epitaxial Graphite: 2D Electron Gas Properties and a Route toward Graphene-based Nanoelectronics,” *J. Phys. Chem. B*, vol. 108, no. 52, pp. 19912–

- 19916, Dec. 2004.
<http://dx.doi.org/10.1021/jp040650f>.
- [11] L. Chen, Y. Tang, K. Wang, C. Liu, and S. Luo, "Direct electrodeposition of reduced graphene oxide on glassy carbon electrode and its electrochemical application," *Electrochem. commun.*, vol. 13, no. 2, pp. 133–137, Feb. 2011.
<http://dx.doi.org/10.1016/j.elecom.2010.11.033>.
- [12] J. Shi, X. Li, G. He, L. Zhang, and M. Li, "Electrodeposition of high-capacitance 3D CoS/graphene nanosheets on nickel foam for high-performance aqueous asymmetric supercapacitors," *J. Mater. Chem. A*, vol. 3, no. 41, pp. 20619–20626, 2015.
<http://dx.doi.org/10.1039/C5TA04464B>.
- [13] A. Di Luca et al., "Gradients in pore size enhance the osteogenic differentiation of human mesenchymal stromal cells in three-dimensional scaffolds," *Sci. Rep.*, vol. 6, p. 22898, Mar. 2016.
<http://dx.doi.org/10.1038/srep22898>.
- [14] C. M. Murphy and F. J. O'Brien, "Understanding the effect of mean pore size on cell activity in collagen-glycosaminoglycan scaffolds," *Cell Adh. Migr.*, vol. 4, no. 3, pp. 377–381, Dec. 2010.
<http://dx.doi.org/10.4161/cam.4.3.11747>.
- [15] P. Kasten, I. Beyen, P. Niemeyer, R. Luginbühl, M. Böhner, and W. Richter, "Porosity and pore size of β -tricalcium phosphate scaffold can influence protein production and osteogenic differentiation of human mesenchymal stem cells: An in vitro and in vivo study," *Acta Biomater.*, vol. 4, no. 6, pp. 1904–1915, Nov. 2008.
<http://dx.doi.org/10.1016/j.actbio.2008.05.017>.
- [16] L. D. Guillen-Romero et al., "Synthetic hydroxyapatite and its use in bioactive coatings," *J. Appl. Biomater. Funct. Mater.*, vol. 17, no. 1, 2019.
<http://dx.doi.org/10.1177/2280800018817463>.
- [17] J. Wosek, "Fabrication of Composite Polyurethane/Hydroxyapatite Scaffolds Using Solvent-Casting Salt Leaching Technique," *Advances in Materials Science*, vol. 15, p. 14, 2015. <http://dx.doi.org/10.1515/adms-2015-0003>.
- [18] S. Frago Angeles, R. Vera-Graziano, G. L. Pérez González, A. L. Iglesias, L. E. Gómez Pineda, and L. J. Villarreal-Gómez, "Síntesis y Caracterización de Hidroxiapatita Sintética para la Preparación de Filmes de PLGA/HAP con Potencial Uso en Aplicaciones Biomédicas," *ReCIBE*, vol. 7, no. 2, pp. 93–116, 2018.
<http://recibe.cucei.udg.mx/ojs/index.php/ReCIBE/article/view/94>.
- [19] S. Koutsopoulos, "Synthesis and characterization of hydroxyapatite crystals: a review study on the analytical methods". *J Biomed Mater Res*. Vol. 62, Pp. 600–612, 2002.
<https://doi.org/10.1002/jbm.10280>
- [20] A.F. Khan, M. Awais, A.S. Khan, "Raman spectroscopy of natural bone and synthetic apatites". *Appl Spectrosc Rev*. Vol. 48, Pp. 329–355, 2013.
<https://doi.org/10.1080/05704928.2012.721107>
- [21] G.R. Sauer, W.B. Zunic, J. R. Durig, "Fourier transform Raman spectroscopy of synthetic and biological calcium phosphates". *Calcif Tissue Int*. Vol. 54, Pp. 414, 1994.
<https://doi.org/10.1007/BF00305529>
- [22] A.-J. Wang et al., "Effect of sintering on porosity, phase, and surface morphology of spray dried hydroxyapatite microspheres," *J. Biomed. Mater. Res. Part A*, vol. 87A, no. 2, pp. 557–562, 2008, <http://dx.doi.org/10.1002/jbm.a.31895>.
- [23] S. V Dorozhkin, "Calcium orthophosphate deposits: Preparation, properties and biomedical applications," *Mater. Sci. Eng. C*, vol. 55, pp. 272–326, Oct. 2015, doi: <http://dx.doi.org/10.1016/j.msec.2015.05.033>.
- [24] C. F. C. Brown, J. Yan, T. T. Y. Han, D. M. Marecak, B. G. Amsden, and L. E. Flynn, "Effect of decellularized adipose tissue particle size and cell density on adipose-derived stem cell proliferation and adipogenic differentiation in composite methacrylated chondroitin sulphate hydrogels," *Biomed. Mater.*, vol. 10, no. 4, p. 45010, 2015, <http://dx.doi.org/10.1088/1748-6041/10/4/045010>.
- [25] D. N. Misra, *Adsorption on and Surface Chemistry of Hydroxyapatite*. Springer US, 2013.

<https://books.google.com.mx/books?id=uDHvBwAAQBAJ>.

[26] M. Morgia, Z. Adamczyk, and M. Oćwieja, “Stability of silver nanoparticle monolayers determined by in situ streaming potential measurements,” *J. Nanoparticle Res.*, vol. 15, no. 11, p. 2076, Oct. 2013. <http://dx.doi.org/10.1007/s11051-013-2076-5>.

[27] P. de Vos, B. J. de Haan, J. A. A. M. Kamps, M. M. Faas, and T. Kitano, “Zeta-potentials of alginate-PLL capsules: A predictive measure for biocompatibility?” *J. Biomed. Mater. Res. Part A*, vol. 80A, no. 4, pp. 813–819, 2007. <http://dx.doi.org/10.1002/jbm.a.30979>.

[28] D. Malina, K. Biernat, and A. Sobczak-Kupiec, “Studies on sintering process of

synthetic hydroxyapatite,” *Acta Biochim. Pol.*, vol. 60, no. 4, pp. 851–855, 2013.

http://www.actabp.pl/pdf/4_2013/851.pdf.

[29] J. González Ocampo, D. M. Escobar Sierra, and C. P. Ossa Orozco, “Métodos de fabricación de cuerpos porosos de hidroxiapatita, revisión del estado del arte,” *Revista ION*, vol. 27. scieloco, pp. 55–70, 2014.

<https://revistas.uis.edu.co/index.php/revistaion>

[30] M. Sadat-Shojai, M.-T. Khorasani, E. Dinpanah-Khoshdargi, and A. Jamshidi, “Synthesis methods for nanosized hydroxyapatite with diverse structures,” *Acta Biomater.*, vol. 9, no. 8, pp. 7591–7621, Aug. 2013.

<http://dx.doi.org/10.1016/j.actbio.2013.04.012>.



Este texto está protegido por una licencia [Creative Commons 4.0](https://creativecommons.org/licenses/by/4.0/)

Usted es libre para Compartir —copiar y redistribuir el material en cualquier medio o formato— y Adaptar el documento —remezclar, transformar y crear a partir del material— para cualquier propósito, incluso para fines comerciales, siempre que cumpla la condición de:

Atribución: Usted debe dar crédito a la obra original de manera adecuada, proporcionar un enlace a la licencia, e indicar si se han realizado cambios. Puede hacerlo en cualquier forma razonable, pero no de forma tal que sugiera que tiene el apoyo del licenciante o lo recibe por el uso que hace de la obra.

[Resumen de licencia - Texto completo de la licencia](#)